

# Synthesis of Biodiesel using the Mg/Al/Zn Hydrotalcite/SBA-15 Nanocomposite Catalyst

Marimuthu Prabu,<sup>†,‡</sup> Marimuthu Manikandan,<sup>§</sup> Prabu Kandasamy,<sup>†,‡</sup> P. R. Kalaivani,<sup>||</sup> Nagappan Rajendiran,<sup>\*,†,‡</sup> and Thirumalaiswamy Raja<sup>\*,†,‡</sup>

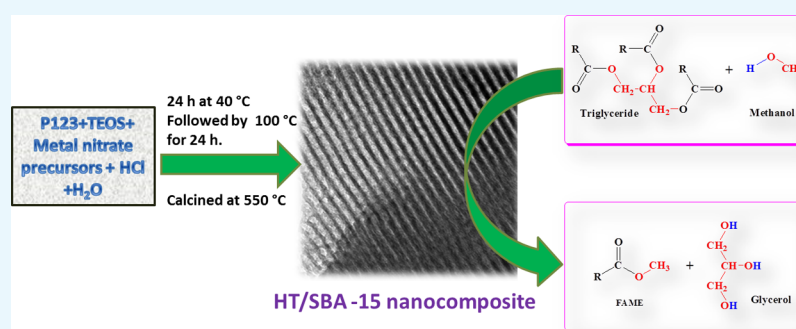
<sup>†</sup>Catalysis and Inorganic Chemistry Division, CSIR-National Chemical Laboratory, Dr. HomiBhabha Road, Pune 411 008, India

<sup>‡</sup>Academy of Scientific and Innovative Research (AcSIR), Ghaziabad 201002, India

<sup>§</sup>Department of Chemistry, School of Advanced Sciences, VIT, Vellore 632014, India

<sup>||</sup>Bharathi Women's College, George Town, Chennai, Tamil Nadu 600108, India

<sup>†</sup>Department of Polymer Science, University of Madras, Guindy Campus, Chennai 600025, Tamil Nadu, India



**ABSTRACT:** Biodiesel production is an enchanting and eccentric pathway for the reduction of use of fossil fuels and is procured from biologically available renewable sources such as oils and fats. A novel Mg/Al/Zn-based hydrotalcite/SBA-15 composite material having a high catalytic activity was developed and investigated for the transesterification of vegetable oil. The rationally developed composites were systematically characterized and assessed in the transesterification of soybean oil in the presence of methanol. The physicochemical evaluation of the nanocomposites demonstrated the influence of Zn in the textural characteristics, density of the basic sites, and successively the catalytic activity. The catalytic efficiency of the MAZ-*x*/SBA-15 composite could be linked with the basic site density determined by the temperature-programmed desorption of CO<sub>2</sub>. Among all the composites used, the MAZ-1/SBA-15 nanocomposite showed the highest activity for biodiesels, with a yield of around 90% under economical reaction conditions. The catalytic studies conferred that the fatty acid methyl ester yield is significantly influenced by various experimental conditions such as the catalyst molar ratio, reaction temperature, pressure, and contact time. It was also found that the incorporation of hydrotalcite into SBA-15 pore channels can enhance the catalyst efficiency and stability of the nanocomposite. Moreover, under mild reaction conditions, a remarkably stable catalytic performance was achieved for more than 200 h of time on stream with no catalyst deactivation.

## 1. INTRODUCTION

World's energy resources mainly rely on coal, oil, microalgae, and natural gas. However, these resources are limited, due to which biofuels are used as a renewable energy resource in reducing environmental pollution and the concern about the medium and long-term supply of fossil fuels.<sup>1–3</sup> The global need of biodiesel is enormously increased owing to its environmental benefits, and the worldwide production of biodiesel reached 140 billion liters in 2017.<sup>4,5</sup> Biodiesel is generally produced from the methanolysis of triglycerides with low-molecular-weight alcohols and is analogous to the composition and combustion behavior of fossil fuels.<sup>6</sup> Chemically, it consists mostly of fatty acid methyl esters (FAMEs), and their physicochemical properties such as energy content, cetane number, and viscosity are similar to those of

petroleum-based diesel fuels. Thus, biodiesel can be used in compression–ignition engines with little or no modifications. Additionally, biodiesel with different concentrations of blend is the interesting option to get high performance of cetane number and lubricity.<sup>7</sup> The remarkable advantage of biodiesel as a fuel additive is the suppression of NO<sub>x</sub>, CO, sulfur, and polyaromatic hydrocarbons, consequently causing less impact on the environment.<sup>1</sup>

The industrial process for the biodiesel production commonly employed homogeneous base catalysts such as sodium or potassium hydroxides for the transesterification of

**Received:** September 27, 2018

**Accepted:** January 4, 2019

**Published:** February 18, 2019

animal fats or plant oils with short-chain alcohols, usually methanol, because of a high percentage of conversion rates. However, the use of the aforementioned catalysts renders tedious process and demands purification steps to remove the surplus glycerol and catalyst. Also, the occurrence of undesired saponification reaction implies the massive production of toxic wastes and leads to reduce the conversion rate and make a complicated process.<sup>6</sup> However, these problems can be resolved by the replacement of homogeneous catalysts by heterogeneous solid base ones.<sup>8</sup> The employment of heterogeneous solid base catalysts in the transesterification reaction paves several advantages such as reduction of undesirable saponification reaction, process simplification, cost-effectiveness by minimizing the number of operations, and easier adaptation to continuous processes. Also, glycerol obtained as a byproduct over transesterification of plant oils exhibits a better quality compared to homogeneous catalyst systems.<sup>9</sup> On the other hand, the use of solid acid catalysts for the biodiesel production is also studied. Although there are a lot of reports to produce the high efficiency of biodiesel from the acid, inorganic–organic hybrid, and immobilized catalysts, the demand of biodiesel increased drastically.<sup>10</sup> Over the past few decades, the search of a successful catalyst for the efficient FAME production has attained a greater interest in both industries and academia. A wide range of results have been reported using alkali and alkaline earth metal oxides for the conversion of vegetable oils to FAME.<sup>11,12</sup> Pasupulety et al. reported 90% yield of FAME via transesterification of soybean oil (SBO) by batch mode using coprecipitated Mg–Zn mixed oxides.<sup>13</sup> Bazargan et al. utilized CaO as a base catalyst for the transesterification of sunflower oil with almost 99% conversion.<sup>14</sup> The leaching of alkali metal ions leads to the catalyst deactivation and suppresses the quality of the obtained biodiesel.<sup>15</sup> Therefore, for the development of green and efficient solid bases, researchers were focused on the structured and stable metal oxide frameworks as the catalyst for the transesterification reaction.

Hydrotalcites (HTs), a class of anionic clays, are the extensively studied solid base oxides resulting with moderate FAME yields. Xie et al. have investigated the performance of Mg/Al HT catalysts for the methanolysis of SBO with the conversion of 67%.<sup>16</sup> Gomes et al. have compared MgAl-lamellar structures treated at different calcination temperatures for the transesterification of SBO with methanol and found that basic sites hold a significant role in the FAME yield.<sup>17</sup> Antunes et al. have used different solid base catalysts such as MgO and Mg/Al mixed oxides for the liquid-phase transesterification reaction, which yield 70–85% of FAME.<sup>18</sup> On the basis of the literature, it is observed that the transesterification performance could be directly related to the density of basic sites present on the catalyst system. Hydrothermally stable silica frameworks such as SBA-15 can be used to annul the drawbacks of solid base catalysts because they offer diverse pore interconnectivities, a wide pore size to minimize the diffusion of reactants, an excellent surface-to-volume ratio, huge surface area, and thermal stability.<sup>19–21</sup> Moreover, lack of Brønsted acidity on SBA-15 allows tuning the acidity of pure SBA-15 to control the cracking activities.<sup>22</sup> In this context, Creasey et al. developed a hierarchically ordered macroporous–mesoporous SBA-15 template with HT coatings for the base-catalyzed transesterification of glycerol-triolein.<sup>23</sup>

In this study, efforts were made to apply a methodology to fabricate catalytically active Mg/Al/Zn-based HT incorporated on SBA-15 via a versatile in situ method consisting synthesis of macroporous HT-derived oxides comprising ordered silica architectures. This novel methodology opens up the way to a new class of heterogeneous solid bases reinforced upon the highly modifiable interconnectivity and porosity afforded by the underlying silica framework structure. The resulting HT/SBA-15 nanocomposite combines the high surface area and excellent mass-transport characteristics of the parent silica, tunable basicity, and transesterification performance of a pure HT, which result in excellent FAME yield.

## 2. EXPERIMENTAL SECTION

**2.1. In Situ Synthesis of the HT/SBA-15 Nanocomposite.** The mesoporous SBA-15 was synthesized according to the reported literature.<sup>24,25</sup> The HT/SBA-15 composite was prepared as follows: 0.2 g triblock copolymer (EO<sub>20</sub>PO<sub>70</sub>EO<sub>20</sub>) and a calculated amount of Mg(NO<sub>3</sub>)<sub>2</sub>·6H<sub>2</sub>O, Al(NO<sub>3</sub>)<sub>3</sub>·9H<sub>2</sub>O, and Zn(NO<sub>3</sub>)<sub>2</sub>·6H<sub>2</sub>O were dissolved in 75 mL of 1.6 M HCl, and then 4.25 g of tetraethyl orthosilicate (TEOS) was added dropwise maintaining a temperature of 40 °C, with constant stirring. The molar ratio of the mixture P123/TEOS/Zn(NO<sub>3</sub>)<sub>2</sub>/Mg(NO<sub>3</sub>)<sub>2</sub>/Al(NO<sub>3</sub>)<sub>3</sub>/HCl/H<sub>2</sub>O was 1:0.02:2x:2x:x:6:192, where *x* is the molar ratio of TEOS to Al(NO<sub>3</sub>)<sub>3</sub> and the *x* values are 0.02, 0.05, 0.08, 0.18, 0.25, and 0.31. The stirring process for the mixed solution was executed for 24 h at 40 °C, followed by treatment at 100 °C for further 24 h. The resultant slurry was evaporated by heating at 80 °C, and then the obtained solid was dried at 80 °C. The final calcination of the product was carried out at 550 °C for 6 h. The obtained nanocomposite materials were denoted as MAZ-*x*/SBA-15, where M, A, and Z stand for magnesium, aluminum, and zinc, respectively, and *x* is the molar ratio of zinc.

**2.2. Material Characterization.** A PAN analytical X'pert Pro dual goniometer diffractometer was used for the collection of powder X-ray diffraction (XRD) data of synthesized composite catalysts. The patterns were recorded with a step size of 0.008 and a scan rate of 0.5° min<sup>-1</sup>. The Cu-55 K $\alpha$  (1.5418 Å) with Ni filter radiation was used for analysis. CO<sub>2</sub>-temperature-programmed desorption (TPD) analyses were carried out in the Micrometrics 2920 instrument. About 50 mg of the calcined material was loaded in a “U” shaped quartz tube and pretreated at 450 °C (5 °C/min ramping) for 2 h using helium as a carrier gas. For analysis, a gas mixture of 10% CO<sub>2</sub> in helium was allowed to adsorb on the sample surface, and desorption was analyzed in a temperature range from 50 to 1000 °C at a ramp rate of 10 °C. Specific surface area and pore characteristics were determined by N<sub>2</sub>-sorption analysis at liquid nitrogen temperature (–196 °C) using Autosorb 1C Quantachrome USA. The Brunauer–Emmett–Teller (BET) equation was applied to measure the surface area from the adsorption branch. Total pore volume and average pore size measurements are collected from Barret, Joyner, and Halenda (BJH) analysis from the desorption branch. High-resolution transmission electron microscopy (HRTEM) micrographs of all nanocomposites materials were obtained using an FEI Tecnai F30 electron microscope operating at 300 kV. For analysis, the finely powdered samples were dispersed in 2-propanol and deposited onto a holey carbon grid, and the resulting dried samples were analyzed for TEM. Mg, Al, Zn, and O core levels were studied with an X-ray photoelectron

spectrometer. The X-ray photoelectron spectroscopy (XPS) profiles of all elements were recorded at the pass energy of 50 eV and further information about the detailed instrumentation can be found elsewhere.<sup>26</sup>

**2.3. Catalytic Test.** Vapor-phase transesterification of SBO with methanol was carried out in a vertical upflow fixed bed reactor. The pelletized (0.5–0.8 mm) 1 mL catalyst was sandwiched between glass wool and ceramic beads in an Inconel reactor. The catalyst was pretreated at 250 °C in the presence of N<sub>2</sub> flow (99.99%, gas hourly space velocity, GHSV 600–2400 h<sup>-1</sup>) controlled by a Brooks make mass flow controller (5850S) for 2 h. The reaction temperature was regulated to desired conditions (180–300 °C) under the same N<sub>2</sub> flow. A suitable stream of SBO (weight hourly space velocity, WHSV 0.6–1.8 h<sup>-1</sup>) was fed continuously along with different methanol contents (oil to methanol ratio 1:5–1:30) by using the high-precision isocratic syringe pump, and the reactor was vaporized. N<sub>2</sub> flow was switched to 1800–3000 GHSV h<sup>-1</sup>. The products were condensed using a chiller, collected regularly at intervals, and separated, and then the same were analyzed by high-pressure liquid chromatography, (PerkinElmer Series 200) with an evaporative light scattering detector and a C-18 Spheri-5 column (length = 250 mm, i.d. = 4.6 mm and particle size = 5 μm).<sup>1</sup>H nuclear magnetic resonance spectroscopy (Bruker AV 200 MHz) was also used to determine the product and to evaluate the FAME yield.<sup>27</sup>

### 3. RESULTS AND DISCUSSION

**3.1. X-ray Diffraction.** XRD patterns of the as-synthesized and calcined nanocomposite materials are shown in Figure 1.

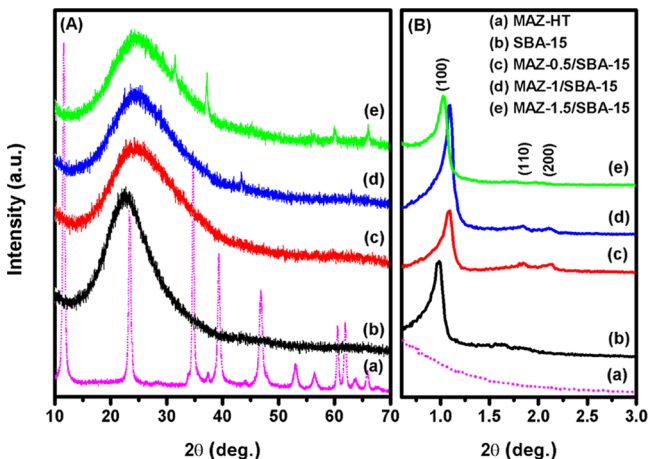


**Figure 1.** (A) Wide-angle and (B) low-angle XRD patterns of the HT, SBA-15, and MAZ-*x*/SBA-15 nanocomposites.

The as-synthesized MAZ-1 HT (a) shows characteristic reflections for the HT features, which evidenced the successful formation of an HT-like structure.<sup>28,29</sup> All calcined MAZ-*x*/SBA-15 composite materials (b–e) exhibit a broad diffuse peak attributed to the noncrystalline silica. The absence of significant reflections of any crystalline phase was detected in the entire pattern even for the high Zn loading, indicating that the HT is located inside the pores of SBA-15. However, small reflections at 31.2° and 36.7° attributable to the ZnO (zincite) phase (JCPDS-36-1451) for the MAZ-1.5/SBA-15 sample conferred that MAZ-1/SBA-15 provides the optimum Zn loading to incorporate the HT structure in the silica

channels.<sup>30</sup> Perceptibly, no pattern corresponding to any mixed oxides in the calcined nanocomposites was observed, which conferred that the HT structure is wholly incorporated into the SBA-15 framework. The small-angle XRD patterns of MAZ-*x*/SBA-15 nanocomposites are depicted in Figure 1B. All samples demonstrate well-resolved reflections that can be indexed to (100), (110), and (200) planes, which correspond to the typical *P6mm* space group, which is in good accordance with SBA-15. These results imply that the framework topology of SBA-15 was retained even after the formation of the composite, indicating that the two-dimensional (2D) hexagonal structure was not altered by the incorporation of HT SBA-15. Moreover, the improved intensity of (100) planes for all HT/SBA-15 samples as compared to parent SBA-15 corroborated that the addition of Mg, Al, and Zn oxides effectively improves the ordered structure.

**3.2. Physicochemical Properties.** The BJH pore size distribution and N<sub>2</sub> adsorption–desorption isotherms of MAZ-*x*/SBA-15 nanocomposites are shown in Figure 2. All

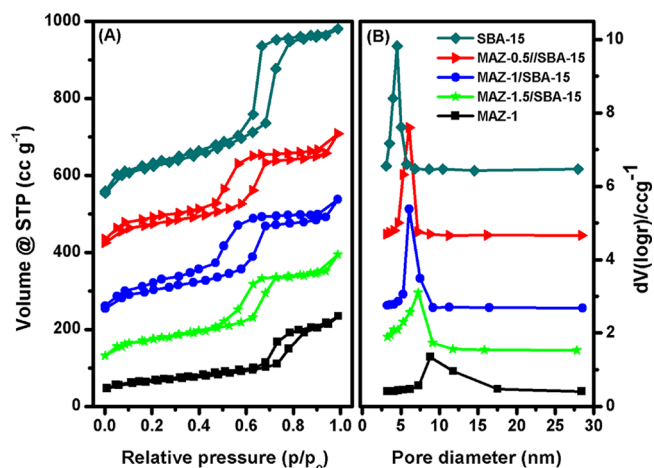


**Figure 2.** (A) N<sub>2</sub> adsorption–desorption isotherm plots and (B) pore size distribution of the HT/SBA-15 nanocomposites.

nanocomposites show type IV isotherm defined by IUPAC classification with H-1 hysteresis loops, which are very similar to SBA-15. Moreover, the hysteresis loops represents the N<sub>2</sub> capillary condensation and high relative pressure that is the characteristic of mesostructures with 2D hexagonal structures.<sup>31</sup> The pore size distribution (Figure 2B) proved that the pores present a cylindrical form in the range of 5–10 nm in size and exists in a narrow size distribution. Furthermore, no considerable alteration in the isotherm type was observed, suggesting that mesoporous cylinder channels are highly ordered and sustained during the formation of MAZ/HT structures inside the SBA-15 framework. These observations are highly consistent with the procured results from the low-angle XRD analysis. The textural properties of the nanocomposite are listed in Table 1, and pure SBA-15 exhibited the BET surface area of about 366 m<sup>2</sup>/g and it is monotonously decreased as the Zn loading increases in the HT structure. This observation further evidences the location of HT-derived mixed metal oxides at SBA-15 channels. However, the successful retention of the average pore diameter up to the MAZ-1.5/SBA-15 sample conferred the uniform dispersion of mixed oxide species.

**Table 1. Physicochemical Properties of Synthesized Catalysts**

s. no.	sample	surface area <sup>a</sup> (m <sup>2</sup> g <sup>-1</sup> )	total pore volume <sup>b</sup> (cm <sup>3</sup> /g)	average pore diameter <sup>b</sup> (nm)	basic sites <sup>c</sup> (mmol g <sup>-1</sup> )
1	SBA-15	366.0	0.71	7.2	n.d
2	MA/SBA-15	312.4	0.60	6.4	0.21
3	MAZ-0.5/SBA-15	285.3	0.49	6.1	0.19
4	MAZ-1/SBA-15	275.5	0.48	6.2	0.18
5	MAZ-1.5/SBA-15	237.3	0.45	4.3	0.15
6	MAZ-1 HT	150.5	0.33	8.8	0.33
7	Zn/SBA-15	312.6	0.62	0.64	n.d

<sup>a</sup>Obtained by BET surface area analysis. <sup>b</sup>Calculated from BJH pore size analysis. <sup>c</sup>Obtained by CO<sub>2</sub>-TPD experiments.

**3.3. Transmission Electron Microscope.** Figure 3 shows the TEM micrographs of SBA-15 and MAZ-1/SBA-15

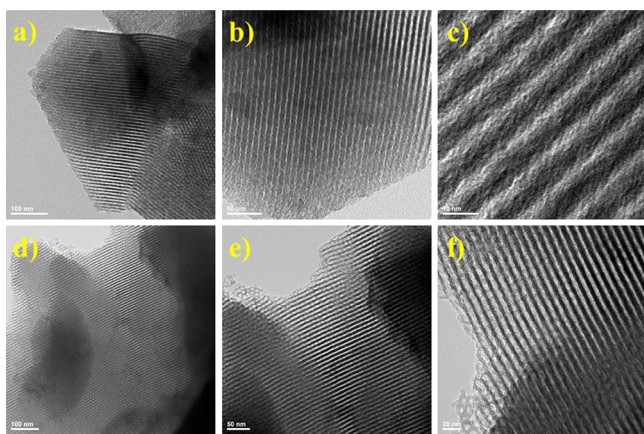


**Figure 3.** TEM micrographs of (a–c) SBA-15 and (d–f) MAZ-1/SBA-15 nanocomposites.

nanocomposites. TEM micrographs (Figure 3a–c) depict the hexagonally arranged cylindrical pores of the ordered structure of SBA-15.<sup>24,32</sup> The TEM micrograph of MAZ-1/SBA-15 also shows characteristic pore channels of the SBA-15 tubular structure (d–f). However, the inherent morphology and distribution of MAZ-1 mixed oxides of the SBA-15 pore channels could not be clearly observed owing to the low scattering contrast between the SBA-15 pore walls and mixed oxides. Furthermore, no lattice fringes corresponding to MgAlZnO<sub>x</sub> mixed oxides were observed outside of SBA-15, which proved that the mixed oxides are inside the pore channels and not agglomerated on the SBA-15 surface.

**3.4. CO<sub>2</sub>-Temperature-Programmed Desorption.** The basic site density of the composite materials was evaluated by CO<sub>2</sub>-TPD, and the obtained results are shown in Figure 4. As shown in the figure, two desorption regions are observed for MAZ-1 HT and MAZ-*x*/SBA-15 nanocomposites. The desorption temperature at 188.4 °C was assigned to the weak basic sites and that of 654.6 °C portrays the combination of medium plus strong basic sites. The origin of weak and strong basic sites was ascribed to the presence of OH<sup>-</sup> and O<sup>2-</sup> species, respectively, which can be coined as Brønsted- and Lewis-type basic sites.<sup>33,34</sup> Broad desorption branches at the temperature range of around 550–700 °C for all samples emphasized that the moderate basicity was present in a major amount.<sup>23</sup> By increasing Zn loading, it can be seen that the profile shift toward low temperature for weak basic sites was observed. The major shift (~40 °C) in desorption peak and broadening in the moderate basicity region were observed for MAZ-1.5/SBA-15, which evidence that the addition of Zn

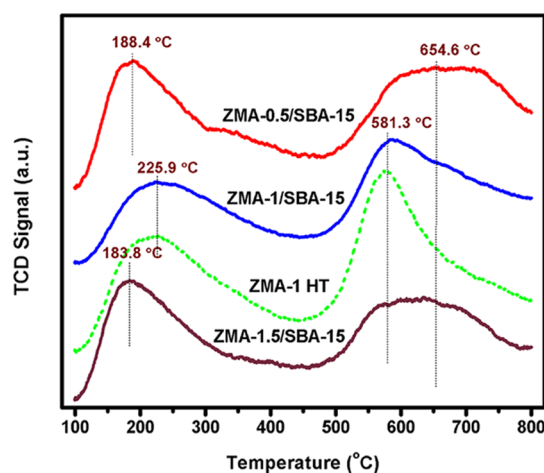


**Figure 4.** CO<sub>2</sub>-TPD of the MAZ-1 HT and ZMA-*x*/SBA-15 nanocomposites.

suppressed the strong basic sites and preserves the moderate basicity. CO<sub>2</sub>-TPD of MAZ-1 HT was used for comparison, which showed the symmetrical profile at similar desorption branches as SBA-15 containing composites. Furthermore, the calculated basic site density listed in Table 1 exhibited the highest basic strength of about 0.33 mmol/g for MAZ-1 HT, and the nanocomposite showed a decreasing trend with respect to the addition of Zn loading. The CO<sub>2</sub>-TPD results concluded that the incorporation of Zn<sup>2+</sup> on Mg/Al layers reduces the formation of OH<sup>-</sup> and O<sup>2-</sup> ions, consequently tuning basic site distribution.

**3.5. X-ray Photoelectron Spectroscopy.** To underpin the additional insights in the MAZ-1 and MAZ-*x*/SBA-15 nanocomposite, XPS analysis was employed. Figure 5 depicts the XPS core-level spectra of the MAZ-1 HT and MAZ-1/SBA-15 nanocomposite. The XPS binding energy values around 1022, 50, 74.2, and 531.8 eV were detected, which were assigned for the peaks of Zn 2p, Mg 2p, Al 2p, and O 1s core levels, respectively.<sup>23,26</sup> The peak at the binding energy of 102.3 eV is originated from Si 2p, from silica in SBA-15.<sup>31</sup> The O 1s asymmetric peak centered at 531.8 eV showed the availability of more than one chemical state for oxygen species. For the MAZ-1 sample, the O 1s peak at 531.7 eV can be credited to the oxygen in pure ZnO.<sup>2</sup> On the other hand, the O 1s profile of the nanocomposite exhibits a symmetric peak at 532.1 eV, which can be attributed to the surface oxygen species of SBA-15. Notably, the O 1s profile of the nanocomposite shows a slightly higher binding energy than MAZ-1, suggesting that the oxygen species are detected from the silica walls of SBA-15.<sup>22</sup> The XPS results of Zn 2p (Figure 5c) with satellite peaks of around 1045.3 eV confirm that Zn exists as ZnO in the MAZ-1/SBA-15 nanocomposite. Interestingly, the ob-

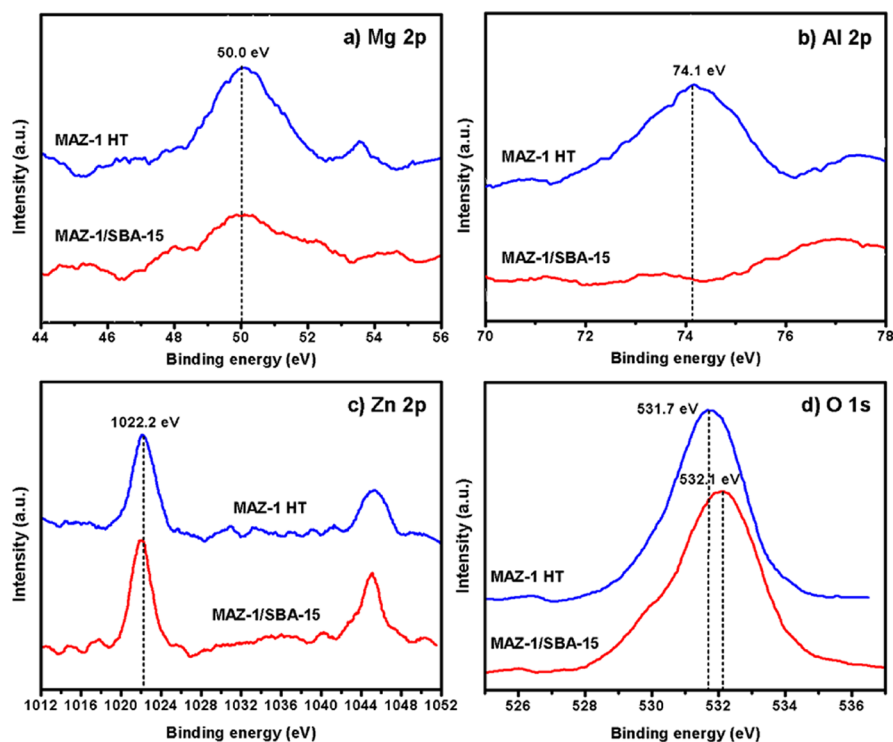


Figure 5. XPS profiles of SBA-15 and MAZ-1/SBA-15 nanocomposites.

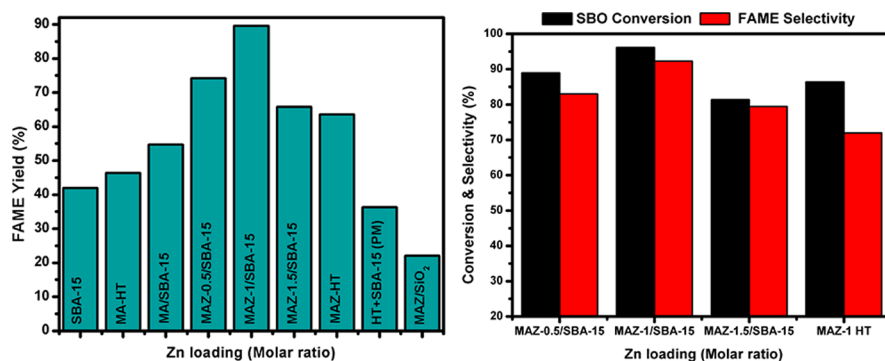


Figure 6. FAME yield (left) and conversion selectivity (right) of various MAZ-*x*/SBA-15 nanocomposites. Reaction conditions: 200 °C, WHSV 1.2 h<sup>-1</sup>, 20 bar pressure, and the ratio of oil to methanol is 1:20.

served spectra for both Mg 2p and Al 2p (Figure 5a,b) are very less in intensity or uninterpretable even after 10 scans for MAZ-1/SBA-15. Because XPS is a surface technique, we can conclude that both Mg and Al are not on the surface, which strongly suggests that the Mg and Al species are probably located within the SBA-15 channels. These results provide critical information about the strong interaction between Mg, Al ions, and SBA-15. This could be the reason for strong basicity observed from CO<sub>2</sub>-TPD experiments. Meanwhile, the presence of Zn on the SBA-15 surface is probably the repulsion between the two acidic centers.

**3.6. Catalytic Activity.** **3.6.1. Optimization of Zn Loading.** The influence of the molar ratio of Zn/Mg/Al in biodiesel was studied at 225 °C, 20 bar N<sub>2</sub> pressure, the oil to methanol ratio was taken as 1:20, and WHSV was maintained at 1.2 h<sup>-1</sup>. The results in Figure 6 showed that the FAME yield has improved with an increase in Zn content from 74.2 to 89.6%. Maximum FAME yield was obtained over the MAZ-1/SBA-15 catalyst, which is almost equal to 90%. However,

increase in Mg or decrease in Zn content in the Mg/Al/Zn molar ratio rendered the decline in the catalytic activity, and the respective yield of the biodiesel was 66% observed for the MAZ-1.5/SBA-15 catalyst. The decrease in activity was due to the partial shielding of Mg–O pairs by the formation of amorphous Al–O structure on the surface, which suppressed the concentration of surface O<sup>2-</sup>, Lewis basic sites.<sup>16</sup> To fathom the role of MAZ-1/SBA-15 nanocomposites on the transesterification of SBA-15, the MAZ-1 catalyst was subjected for catalytic activity under optimized reaction conditions. The observed results in Figure 6 showed a moderate conversion and less selectivity and the activity of MAZ-1 might be due to the existence of surface basic sites, which was verified from the CO<sub>2</sub>-TPD results.<sup>18</sup> Remarkably, the highest FAME yield of about 90% was achieved over the MAZ-1/SBA-15 composite, which conferred the presence of optimized surface basicity, which can be attributed to the dissolution of more amounts of MgO in the surface introducing basicity. Also, the Zn<sup>2+</sup> ions in the Mg<sup>2+</sup> lattice,

the acidic centers submerges in the basic matrix may result in concomitant acidic–basic centers and more in the presence of optimum amount of Lewis basicity in the nanocomposites.<sup>17</sup> From the literature, the main factors that influence the transesterification activity are alkalinity and type of basic strength on the catalysts.<sup>19,20</sup> The linearity between total basicity and FAME yield was slightly swerved. MAZ-1.5/SBA-15 with a less amount of basicity was found to yield 65% of biodiesel, which indicated lower influencing nature of lower basic strength in the transesterification rate. In the case of MAZ-1/SBA-15 and HT with MAZ-0.5/SBA-15 the appropriate value of basic strength, the FAME yield was higher than the latter. Through comparison, it can be concluded that both acidic sites and basic sites equally influence the yield of biodiesel. Precisely, either the excess of Zn or Mg content will decrease the yield of biodiesel because of generation of surplus surface acid–base sites. In addition, Al and Zn also contribute acidic sites for biodiesel production from SBO.

On the other hand, the observed results suggested that SBA-15 does not have a significant role in the conversion of triglyceride biodiesel, but it affects the selectivity of the FAME. Because of the high surface area of SBA-15, it favors good dispersion of catalytically active centers and mass-transfer advantages. This also states that MAZ-1/SBA-15 shows high conversion and selectivity (~93%) compared to HT-derived MAZ-1 and paves high stability for the catalyst. SBA-15 acts as an accessible channel to transport SBO components to active sites present at the surface of MAZ-1, thereby promoting high selectivity.

**3.6.2. Effect of Reaction Temperature.** The outcome of reaction temperature on the FAME yield was investigated within the temperature ranging from 200 to 275 °C at WHSV 1.2 h<sup>-1</sup>, 20 bar N<sub>2</sub> pressure, the ratio of oil to methanol was 1:20, and the corresponding results are portrayed in Figure 7.

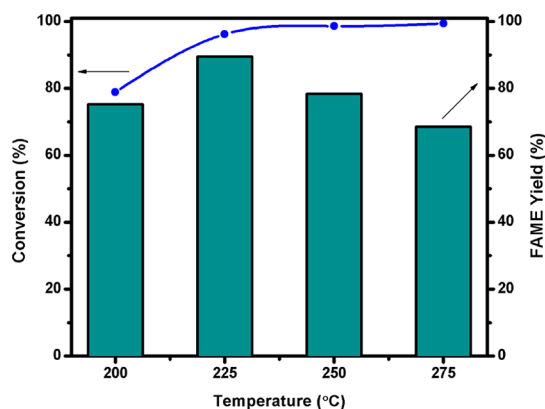


**Figure 7.** Effect of reaction temperature on the transesterification studies over the MAZ-1/SBA-15 catalyst. Reaction conditions: WHSV 1.2 h<sup>-1</sup>, 20 bar and ratio of oil to methanol is 1:20.

The results clearly emphasized that the FAME yield is highly influenced by the reaction temperature because of kinetics. By increasing the reaction temperature, a monotonous decrease in the FAME yield was observed. The reaction temperature affects the viscosity of the SBO inversely; an increase in temperature enhances the miscibility between methanol and oil, in turn leading to a high conversion of triglycerides. Through analysis of reaction progress, it was noted that even after 20 h, the yield of biodiesel at 200, 250, and 275 °C becomes 55, 64, and 56%, respectively. At 225 °C, the FAME

yield of about 89.6% was achieved, which is highest among all the temperatures employed. The volume of the reaction mixture was significantly reduced on performing the reaction at 275°. Beyond 250 °C, there was rapid vaporization of methanol, forming a substantial amount of bubbles to form a foam that results in low FAME yield. In general, the low reaction temperature leads to low reaction results, whereas a higher reaction temperature leads to excessive methanol loss due to evaporation. By considering the safety and cost, the yield of biodiesel was found to be the optimum temperature at 225 °C.

**3.6.3. Effect of Pressure.** The effect of pressure on the transesterification of SBO was investigated at 225 °C, the molar ratio of methanol-to-oil was 20:1, and the results are presented in Figure 8. At lower pressure (10 bar), the FAME

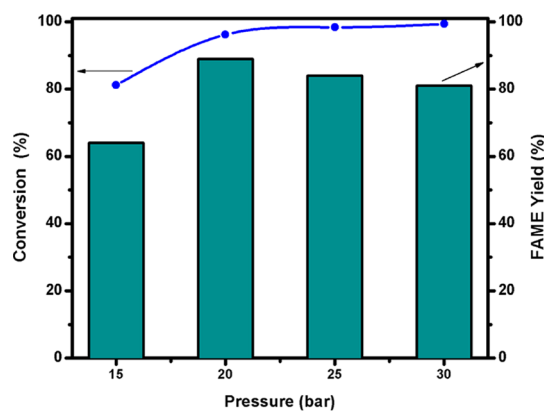


**Figure 8.** Effect of reaction pressure on the transesterification studies over the MAZ-1/SBA-15 catalyst. Reaction conditions: 225 °C, WHSV wrt 1.2 h<sup>-1</sup> ratio of oil to methanol is 1:20.

yield was 65.8%, whereas the pressure increased to 20 bar FAME yield that also increased to 89.6%. Further increment in the pressure had no significant relationship with the FAME yield. However, by growing the pressure to 30 bar leads to the decrease in the FAME yield. Besides, the conversion is increased as the temperature increases, evidencing that the high pressure enhances the conversion but leads to poor selectivity. Also at higher pressure, the fluid density is high, which provides a favorable condition for the interaction between molecules, leading to higher conversion. In this study, the pressure is optimized to 20 bar to achieve the highest FAME yield, which is the lowest among the literature as well as industry (>50 bar).

**3.6.4. Effect of Contact Time.** The catalyst has great influence on the speed of transesterification reaction of SBO. A fixed mole to mole ratio of oil to methanol was set to 1:20, the temperature was set at 225 °C, the pressure was set at 20 bar, and WHSV was varied from 0.6 to 1.8 h<sup>-1</sup>. The effect of WHSV on the yield of biodiesel was scrutinized, and the result is shown in Figure 9. The obtained results showed that WHSV greatly altered the yield of FAME especially in the initial stage of the reaction. The increase in yield with the increase of WHSV can be associated with the information that as the catalyst loading increases the number of active sites increases, thereby attaining an equilibrium within a shorter time. The yield of biodiesel was 64% at 0.6 h<sup>-1</sup> WHSV. At 1.2 h<sup>-1</sup> WHSV, the maximum FAME yield of around 89.6% was reached and the further increase of the WHSV implies a drastic decrease in the yield (59%). The data imply that an optimum

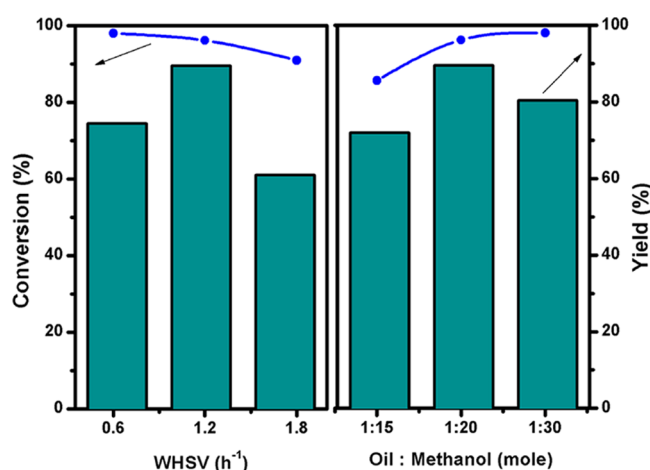


**Figure 9.** Effect of contact time on the transesterification studies over the MAZ-1/SBA-15 catalyst. Reaction conditions: 225 °C and 20 bar pressure.

ratio between reactant molecules and the catalyst amount paves an enhancement in the FAME yield. An increase in the mass-transfer resistance in the multiphase is contributed by the viscous reaction mixture because of the higher amount of reactants. According to stoichiometry, 3 mol of methanol is to be reacted with 1 mol of oil for the production of 3 mol of FAME and 1 mol of glycerol; however, a higher feed mole ratio is required such that the transesterification is more prone toward the desired products. The reaction conditions are 225 °C and 20 bar and different oil to methanol ratios such as 1:15, 1:20, and 1:30. The results shown in Figure 9 convey a considerable increase in the yield of biodiesel with definite increase in oil to methanol ratio to attain 89.6% with a molar ratio of 1:20. However, further increment in the ratio showed a decrease in the yield. This decrement in conversion could be due to the favorableness of triglyceride conversion to monoglycerides with excess methanol. Optimization studies concluded that the low concentration of ratio required a longer time to attain equilibrium according to the kinetics and high ratio will lead to difficulties in separation, which hinders the process because of gravity which leads to decrease in yield. The reaction time can be shortened by the higher ratio to SBO.

**3.6.5. Time on Stream.** The establishment of robustness of the nanocomposite catalysts, the reaction was constantly carried out for longer reaction time (200 h) and the activity was compared with pure SBA-15 and MAZ-1 catalysts, and the obtained results are depicted in Figure 10. As shown in the figure, both MAZ-1 and SBA-15 gave almost 65 and 43% of the FAME yield, respectively, in the initial hours. It could be seen that the drastic decrease in the FAME yield after 100 h for MAZ-1 and in another case for SBA-15 starts to deactivate after 50 h of time on stream (TOS). On the other hand, the in situ synthesized MAZ-1/SBA-15 showed exceptional stability as compared to others, which does not show any change in FAME yield up to 200 h of TOS owing to its optimized textural properties and basicity. In comparison with the literature, the presented nanocomposite catalyst showed excellent stability, which is derived from the synergetic interaction between the HT/SBA-15 combination.

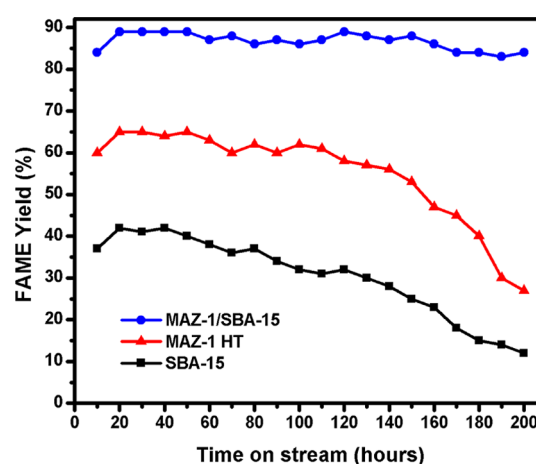


**Figure 10.** Effect of reaction pressure on the transesterification studies over the MAZ-1/SBA-15 catalyst. Reaction conditions: 225 °C, WHSV 1.2 h<sup>-1</sup> wrt SBO, ratio of oil to methanol is 1:20.

## 4. CONCLUSIONS

Synthesis of biodiesel from SBO via transesterification reaction using MAZ-*x*/SBA-15 nanocomposite catalysts has been successfully investigated. Among all employed for catalytic screening, MAZ-1/SBA-15 exhibited the best catalytic performance with almost 90% of FAME yield. The superior catalytic behavior of MAZ-1/SBA-15 can be directly correlated to the presence of optimal amount of moderate surface basic sites. The characterization studies confirmed that the uniform distribution of the HT structure incorporated the pores of SBA-15, providing an excellent activity and stability. Furthermore, the catalytic activity results were compared at different reaction conditions over the optimized catalyst and support has a significant role for the triglyceride conversion. Moreover, the reported catalyst does not show any catalytic deactivation up to 200 h TOS, which allow it to stand as a promising candidate for the future aspects and industrial utilization. This catalyst can be used for the dehydration studies by tuning the acidity.

## AUTHOR INFORMATION

### Corresponding Authors

\*E-mail: [nrajendiar@yahoo.com](mailto:nrajendiar@yahoo.com). Phone: +91-22202823, +91-9176141843 (N.R.).

\*E-mail: [t.raja@ncl.res.in](mailto:t.raja@ncl.res.in). Phone: (+) 91-20-25902006. Fax: (+) 91-20-25902633 (T.R.).

### ORCID

Nagappan Rajendiran: 0000-0002-8903-5132

Thirumalaiswamy Raja: 0000-0002-2487-7363

### Notes

The authors declare no competing financial interest.

## ACKNOWLEDGMENTS

The authors acknowledge DST-SERB and NMITLI from CSIR, New Delhi, for funding and financial support.

## REFERENCES

- (1) Kouzu, M.; Yamanaka, S.-y.; Hidaka, J.-s.; Tsunomori, M. Heterogeneous catalysis of calcium oxide used for transesterification of soybean oil with refluxing methanol. *Appl. Catal., A* **2009**, *355*, 94–99.

- (2) Sivasamy, A.; Cheah, K. Y.; Fornasiero, P.; Kemausor, F.; Zinoviev, S.; Miertus, S. Catalytic Applications in the Production of Biodiesel from Vegetable Oils. *ChemSusChem* **2009**, *2*, 278–300.
- (3) Hassan, M. H.; Kalam, M. A. An Overview of Biofuel as a Renewable Energy Source: Development and Challenges. *Procedia Eng.* **2013**, *56*, 39–53.
- (4) Pradima, J.; Rajeswari Kulkarni, M. Review on enzymatic synthesis of value added products of glycerol, a by-product derived from biodiesel production. *Resour.-Effic. Technol.* **2017**, *3*, 394. International Energy Agency. <https://www.iea.org/tcep/transport/biofuels/> (last updated May 23, 2018).
- (5) Kouzu, M.; Yamanaka, S.-y.; Hidaka, J.-s.; Tsunomori, M. Heterogeneous catalysis of calcium oxide used for transesterification of soybean oil with refluxing methanol. *Appl. Catal., A* **2009**, *355*, 94–99.
- (6) Murugesan, A.; Umarani, C.; Chinnusamy, T. R.; Krishnan, M.; Subramanian, R.; Neduzchezain, N. Production and analysis of biodiesel from non-edible oils-A review. *Renewable Sustainable Energy Rev.* **2009**, *13*, 825–834.
- (7) Hazrat, M. A.; Rasul, M. G.; Khan, M. M. K. Lubricity improvement of the ultra-low sulfur diesel fuel with the biodiesel. *Energy Procedia* **2015**, *75*, 111–117.
- (8) Lee, D.-W.; Park, Y.-M.; Lee, K.-Y. Heterogeneous base catalysts for transesterification in biodiesel synthesis. *Catal. Surv. Asia* **2009**, *13*, 63–77.
- (9) Chai, F.; Cao, F.; Zhai, F.; Chen, Y.; Wang, X.; Su, Z. Transesterification of vegetable oil to biodiesel using a heteropolyacid solid catalyst. *Adv. Synth. Catal.* **2007**, *349*, 1057–1065.
- (10) Saravanan, K.; Tyagi, B.; Shukla, R. S.; Bajaj, H. C. Esterification of palmitic acid with methanol over template-assisted mesoporous sulfated zirconia solid acid catalyst. *Appl. Catal., B* **2015**, *172–173*, 108–115. (a) Xie, W.; Wang, H.; Li, H. Silica-Supported Tin Oxides as Heterogeneous Acid Catalysts for Transesterification of Soybean Oil with Methanol. *Ind. Eng. Chem. Res.* **2011**, *51*, 225–231. (b) Xie, W. L.; Han, Y. X.; Tai, S. N. Biodiesel production using biguanide-functionalized hydroxyapatite-encapsulated- $\gamma$ -Fe<sub>2</sub>O<sub>3</sub> nanoparticles. *Fuel* **2017**, *210*, 83. (c) Xie, W.; Wang, J. Enzymatic Production of Biodiesel from Soybean Oil by Using Immobilized Lipase on Fe<sub>3</sub>O<sub>4</sub>/Poly(styrene-methacrylic acid) Magnetic Microsphere as a Biocatalyst. *Energy Fuels* **2014**, *28*, 2624–2631. (d) WenleiXie; Huang, M. Immobilization of *Candida rugosa* lipase onto graphene oxide Fe<sub>3</sub>O<sub>4</sub> nanocomposite: Characterization and application for biodiesel production. *Energy Convers. Manage* **2018**, *159*, 42.
- (11) Ngamcharussrivichai, C.; Totarat, P.; Bunyakiat, K. Ca and Zn mixed oxide as a heterogeneous base catalyst for transesterification of palm kernel oil. *Appl. Catal., A* **2008**, *341*, 77–85.
- (12) Feyzi, M.; Shahbazi, E. Catalytic performance and characterization of Cs-Ca/SiO<sub>2</sub>-TiO<sub>2</sub> nanocatalysts for biodiesel production. *J. Mol. Catal. A: Chem.* **2015**, *404–405*, 131–138.
- (13) Pasupulety, N.; Rempel, G. L.; Ng, F. T. T. Studies on Mg-Zn mixed oxide catalyst for biodiesel production. *Appl. Catal., A* **2015**, *489*, 77–85.
- (14) Bazargan, A.; Kostić, M. D.; Stamenković, O. S.; Veljković, V. B.; McKay, G. A calcium oxide-based catalyst derived from palm kernel shell gasification residues for biodiesel production. *Fuel* **2015**, *150*, 519–525.
- (15) Liu, Q.; Wang, B.; Wang, C.; Tian, Z.; Qu, W.; Ma, H.; Xu, R. Basicities and transesterification activities of Zn-Al hydrotalcites-derived solid bases. *Green Chem.* **2014**, *16*, 2604–2613.
- (16) Xie, W.; Peng, H.; Chen, L. Calcined Mg-Al hydrotalcites as solid base catalysts for methanolysis of soybean oil. *J. Mol. Catal. A: Chem.* **2006**, *246*, 24–32.
- (17) Gomes, J. F. P.; Puna, J. F. B.; Gonçalves, L. M.; Bordado, J. C. M. Study on the use of MgAl hydrotalcites as solid heterogeneous catalysts for biodiesel production. *Energy* **2011**, *36*, 6770–6778.
- (18) Antunes, W. M.; Veloso, C. d. O.; Henriques, C. A. Transesterification of soybean oil with methanol catalyzed by basic solids. *Catal. Today* **2008**, *133–135*, 548–554.
- (19) Li, Z.; Wei, X.; Ming, T.; Wang, J.; Ngai, T. Dual templating synthesis of hierarchical porous silica materials with three orders of length scale. *Chem. Commun.* **2010**, *46*, 8767–8769.
- (20) Wan, Y.; Zhao, D. On the controllable soft-templating approach to mesoporous silicates. *Chem. Rev.* **2007**, *107*, 2821–2860.
- (21) Zhang, F.; Yan, Y.; Yang, H.; Yan, Y.; Yu, C.; Tu, B.; Zhao, D. Understanding effect of wall structure on the hydrothermal stability of mesostructured silica SBA-15. *J. Phys. Chem. B* **2005**, *109*, 8723–8732.
- (22) Wang, H.; Yan, S.; Salley, S. O.; Simon Ng, K. Y. Support effects on hydrotreating of soybean oil over NiMo carbide catalyst. *Fuel* **2013**, *111*, 81–87.
- (23) Creasey, J. J.; Parlett, C. M. A.; Manayil, J. C.; Isaacs, M. A.; Wilson, K.; Lee, A. F. Facile route to conformal hydrotalcite coatings over complex architectures: a hierarchically ordered nanoporous base catalyst for FAME production. *Green Chem.* **2015**, *17*, 2398–2405.
- (24) Creasey, J. J.; Chierigato, A.; Manayil, J. C.; Parlett, C. M. A.; Wilson, K.; Lee, A. F. Alkali- and nitrate-free synthesis of highly active Mg-Al hydrotalcite-coated alumina for FAME production. *Catal. Sci. Technol.* **2014**, *4*, 861–870.
- (25) Zhao, D.; Feng, J.; Huo, Q.; Melosh, N.; Fredrickson, G. H.; Chmelka, B. F.; Stucky, G. D. Triblock Copolymer Syntheses of Mesoporous Silica with Periodic 50 to 300 Angstrom Pores. *science* **1998**, *279*, 548–552.
- (26) Roy, K.; Vinod, C. P.; Gopinath, C. S. Design and Performance Aspects of a Custom-Built Ambient Pressure Photoelectron Spectrometer toward Bridging the Pressure Gap: Oxidation of Cu, Ag, and Au Surfaces at 1 mbar O<sub>2</sub> Pressure. *J. Phys. Chem. C* **2013**, *117*, 4717–4726.
- (27) Mello, V. M.; Oliveira, F. C. C.; Fraga, W. G.; do Nascimento, C. J.; Suarez, P. A. Z. Determination of the content of fatty acid methyl esters (FAME) in biodiesel samples obtained by esterification using <sup>1</sup>H-NMR spectroscopy. *Magn. Reson. Chem.* **2008**, *46*, 1051.
- (28) Manikandan, M.; Venugopal, A. K.; Prabu, K.; Jha, R. K.; Thirumalaiswamy, R. Role of surface synergistic effect on the performance of Ni-based hydrotalcite catalyst for highly efficient hydrogenation of furfural. *J. Mol. Catal. A: Chem.* **2016**, *417*, 153–162.
- (29) Santhanalakshmi, J.; Raja, T. Selective N-methylation of aniline by calcined MgAl<sub>2</sub>(OH)<sub>6</sub> layered double hydroxides. *Appl. Catal., A* **1996**, *147*, 69–80.
- (30) Veiga, P. M.; Luna, A. S.; de Figueiredo Portilho, M.; de Oliveira Veloso, C.; Henriques, C. A. Zn,Al-catalysts for heterogeneous biodiesel production: Basicity and process optimization. *Energy* **2014**, *75*, 453–462.
- (31) Galarneau, A.; Cambon, H.; Di Renzo, F.; Fajula, F. True microporosity and surface area of mesoporous SBA-15 silicas as a function of synthesis temperature. *Langmuir* **2001**, *17*, 8328–8335.
- (32) dos Santos, S. M. L.; Nogueira, K. A. B.; de Souza Gama, M.; Lima, J. D. F.; da Silva, I. J., Jr.; de Azevedo, D. C. S. Synthesis and characterization of ordered mesoporous silica (SBA-15 and SBA-16) for adsorption of biomolecules. *Microporous Mesoporous Mater.* **2013**, *180*, 284–292.
- (33) Climent, M. J.; Corma, A.; De Frutos, P.; Iborra, S.; Noy, M.; Velly, A.; Concepción, P. Chemicals from biomass: Synthesis of glycerol carbonate by transesterification and carbonylation with urea with hydrotalcite catalysts. The role of acid-base pairs. *J. Catal.* **2010**, *269*, 140–149.
- (34) Corma, A.; Hamid, S.; Iborra, S.; Velly, A. Lewis and Brønsted basic active sites on solid catalysts and their role in the synthesis of monoglycerides. *J. Catal.* **2005**, *234*, 340–347.